Chapter 14
Interaction Between Oxygen and Yttrium Impurity Atoms as well as Vacancies in fcc Iron Lattice: *Ab Initio* Modeling

A. Gopejenko, Yu.F. Zhukovskii, P.V. Vladimirov, E.A. Kotomin, and A. Möslang

Abstract Synthesis of advanced radiation-resistant steels as construction materials for nuclear reactors, which contain the uniformly distributed yttria precipitates (ODS steels), is an important task for ecological security of nuclear plants. The initial stage of theoretical simulation on oxide cluster growth in the steel matrix is a large-scale *ab initio* modeling on pair- and triple-wise interaction between the Y and O impurity atoms as well as Fe vacancies, including their different combinations, in the paramagnetic face-centered-cubic (*fcc*) iron lattice. Calculations on the pair of Y atoms have shown that no bonding appears between them, whereas a certain attraction has been found between Y substitute atom and Fe vacancy. Inter-defect bonding is also formed between the impurity atoms in Y-O and O-O pairs. These calculations have led to the assumption that inclusion of O atom is necessary to form a stable bonding between the impurity atoms, however, the calculations of Y-O-Y defect cluster (where O atom is positioned in the interstitial position), have shown that it is not enough. The main conclusion from these calculations is that the role of Fe vacancies in the inter-defect bonding is quite significant, which was proved by the calculations of Y-O-Y cluster with O atom in the substitute position as well as by the calculations of the Y-V_{Fe}-Y cluster.

Keywords ODS steels • Yttrium oxide precipitates • γ-Fe lattice • DFT calculations • VASP plane-wave code

A. Gopejenko (✉) • Yu.F. Zhukovskii • E.A. Kotomin
Institute of Solid State Physics, University of Latvia, 8 Kengaraga str., LV-1063 Riga, Latvia
e-mail: agopejen@inbox.lv

P.V. Vladimirov • A. Möslang
Forschung, Institut für Materialforschung-I, Institut für Technologie, Karlsruhe, Germany

Y.N. Shunin and A.E. Kiv (eds.), *Nanodevices and Nanomaterials for Ecological Security*, NATO Science for Peace and Security Series B: Physics and Biophysics, DOI 10.1007/978-94-007-4119-5_14,

14.1 Introduction

Reduced activation steels strengthened by yttria precipitates are considered as promising construction materials for fusion- and advanced fission-reactors [1]. In particular, their use for fusion reactor blanket structure would allow increasing the operation temperature by ~100 K [1–3]. The development of the oxide dispersion strengthened (ODS) steels for fission and fusion reactors requires a deep understanding of the mechanism and kinetics of Y_2O_3 cluster precipitation in the steel matrix as nanoparticles size and spatial distribution significantly affect both mechanical properties and radiation resistance of ODS steels [3].

Ferritic-martensitic steels containing Cr with concentration 9–12% used as construction materials for reactors (with mainly wall and blanket applications) have better corrosion/oxidation resistance as compared to the low-Cr steels. These advanced steels are characterized by a noted reduced-activation property that refers to a quick radioactive decay after neutron irradiation, allowing shallow burial of the components after component replacement or plant decommissioning. This property will be helpful in Gen-IV reactors, if not the sole guiding factor. Further, they have good void swelling resistance and relatively good creep resistance. However, there are concerns regarding their low long-term creep rupture strength at higher temperatures and irradiation embrittlement at or less than 400°C [4].

ODS steels are usually produced by mechanical alloying for several tens of hours followed by hot isostatic pressing (HIPping) at temperature around 1,275–1,475 K and at pressure ~100 MPa. To produce the material with improved mechanical properties, better radiation resistance and higher operation temperatures, ODS steels are continuously refined and optimized [1].

The formation mechanism of oxide precipitate particles has not been completely understood yet. A number of TEM studies have been performed on different ODS steels, in order to understand the structure and composition of ODS particles [5, 6]. The main breakthrough of these studies is that a specific orientation relationship between the atomistic structures of Y_2O_3 nanoparticles and the steel matrix has been established. There are experimental evidences that significant part of Y and O atoms are decomposed from yttria clusters in steel matrix with concentrations above their solubility [7–9]. This might mean that the precipitation of Y_2O_3 particles occurs at the hipping stage. Recent experimental studies confirm that minor alloying elements contained in steel matrix can affect chemical composition and dispersion of ODS precipitates [10]. These observations might also support the previous experimental evidences that the dissolution of Y_2O_3 particles occurs during mechanical alloying and subsequent precipitation occurs during hipping [7–9]. This means that the kinetics of the ODS particles growth might be controlled by diffusion of solute atoms.

To perform the modeling of the ODS steels formation, the two-step theoretical approach for atomistic simulation of this process is proposed. During the *first step*, the extensive first-principle calculations on some yttrium and oxygen complexes as well as Fe vacancies inside *fcc* iron lattice were previously performed by us

[11, 12]. From those calculations, both interaction energies between solute and matrix atoms as well as barriers for migration of different solute atoms were particularly extracted for atomistic simulations. In this study, we systematize these parameters for all possible pair- and triple-wise defect interactions in γ-Fe.

During the *second step*, the results of the first-principle calculations will be used to study the precipitate growth using the lattice kinetic Monte Carlo (LKMC) simulations on the matrix and interstitial sublattices. Matrix sublattice is used for iron atoms and substitutional solutes (yttrium), while the oxygen impurity atom can reside both inside the octahedral or tetrahedral interstitial lattice site as well as inside the Fe vacancy. To minimize the system free energy, the direct exchange of metal atoms was considered in recent MC simulations on ODS steels [8]. As mentioned above, the diffusion of precipitating components occurs inside the matrix lattice which leads to structural quasi-coherence of the precipitates with the matrix lattice. With the growth of the precipitates, their bulk energy becomes more substantial than the energy of the matrix-precipitate interface which allows the precipitates both to undergo the phase transition to the more stable phase and to lose their coherence with the matrix.

14.2 Computational Details

To perform *ab initio* modelling in support of the ODS steels formation, the *VASP-4.6* computer code with a plane-wave basis set [13, 14] has been used for the large-scale calculations on both perfect and defective *fcc* lattice of γ-Fe phase. For these parallel calculations with full geometry optimization, the Perdew-Wang-91 non-local exchange-correlation functional within Generalized Gradient Approximation (GGA) [15] and the scalar relativistic Projector-Augmented Wave (PAW) pseudopotentials [16] have been used. The pseudopotentials describe the core electrons of Fe ($4s^1 3d^7$ outer shell), O ($2s^2 2p^4$) and Y ($4s^2 4p^6 5s^1 4d^2$) atoms with 8, 6 and 11 external electrons, respectively. Since at typical temperature range for hot isostatic pressing cubic γ-Fe is known to be paramagnetic, the magnetic effects have not been taken into account in this study.

To define the parameters of calculations reproducing the experimental data (such as lattice constant, bulk modulus and cohesive energy per atom in γ-Fe), a series of preliminary calculations have been performed by us [11]. The analysis of the convergence of the results depending on the supercell size, cut-off energy and the *k*-point mesh in the corresponding Brillouin zone has been also performed. We have confirmed that the numerous calculations on 27-atom $3 \times 3 \times 3$ Fe supercell, performed earlier, are still inaccurate, due to the small size of the supercell which causes the noticeable elastic interactions between the defect and its periodic image. This is the reason why the supercell has been extended up to 64 atoms with the $4 \times 4 \times 4$ enlarged translation vectors of the unit cell.

The cut-off energy has been varied from 300 to 1,200 eV and the *k*-point mesh from 64 ($4 \times 4 \times 4$) to 4,096 ($16 \times 16 \times 16$). It has been found that the calculated

parameters of electronic structure for γ-Fe reliably converge only beginning with the unusually large cut-off energy of 800 eV (*cf.* the default cut-off energy of 267 eV), while varying the *k*-point mesh, it has been found that at least 12 × 12 × 12 mesh allows us to obtain more-or-less plausible results.

In this study, we mainly operate the binding energies for pair- and triple-wise defect configurations. To estimate these energies in presence of A, B and C types of impurity atoms (defects), we have applied the formulae:

$$E^{bind}_{A-B} = E^{form}_{A} + E^{form}_{B} - E^{form}_{A-B}, \tag{14.1}$$

$$E^{bind}_{A-B-C} = E^{form}_{A} + E^{form}_{B} + E^{form}_{C} - E^{form}_{A-B} - E^{form}_{B-C} - E^{form}_{C-A}, \tag{14.2}$$

where $E^{form}_{A} = E^{total}_{lattice+A} - \frac{N-1}{N} E^{total}_{ideal\ lattice} - E_{coh\,A}$ is the formation energy of one A atom in the lattice supercell, $E^{form}_{A-B} = E^{total}_{lattice+AB} - \frac{N-2}{N} E^{total}_{ideal\ lattice} - E_{coh\,AB}$ the formation energy of AB pair, N the number of all the atoms in γ-Fe supercell, $E^{total}_{ideal\ lattice}$, $E^{total}_{lattice+A}$ and $E^{total}_{lattice+AB}$ the total energies of ideal supercell as well as supercell containing either impurity atom A or pair of impurity atoms AB, respectively, while $E_{coh\,A}$ and $E_{coh\,AB}$ the cohesive energies of atom A and AB pair, respectively. If we consider a single Fe vacancy instead of impurity atom, its cohesive energy equals zero. The formation energy of interstitial oxygen impurity atom is: $E^{form}_{A} = E^{total}_{lattice+A} - E^{total}_{ideal\ lattice} - E_{coh\,A}$.

14.3 Main Results

Large-scale calculations on pair-wise defect configurations have been performed beginning with the interactions between the two yttrium substitute atoms (Fig. 14.1) as well as between the Y substitute atom and Fe-vacancy (Fig. 14.2). The results of these calculations are presented in Tables 14.1 and 14.2, respectively. The analysis of the results obtained for interactions between the two Y atoms at different relative distances (1-NN, 2-NN, 3-NN and 4-NN) shows that no bonding exists between them at any inter-atomic distances in *fcc* iron lattice. On the other hand, the largest binding energy in the Y-V_{Fe} pair has been found for the configuration where the Y substitute atom and Fe-vacancy are arranged as the first nearest neighbors (1-NN), *i.e.* this pair is quite stable. A significant relative displacement (1.25 Å) of the Y substitute atom towards the Fe-vacancy has been observed after the relaxation: the former occupies intermediate position between the two empty lattice sites. The binding energy of 0.30 and 0.40 eV has been found between Y atom and Fe-vacancy at 3-NN and 4-NN distances, correspondingly, while the binding energy value between Y atom and Fe vacancy at 2-NN positions is negative. The calculation of the interactions between two Fe vacancies presented in Table 14.3 show that there is practically no binding energy between them at any distance.

The calculations on binding energies between either Y and O substitute atoms or two O substitute atoms (arranged analogously to Fig. 14.1) have been also performed.

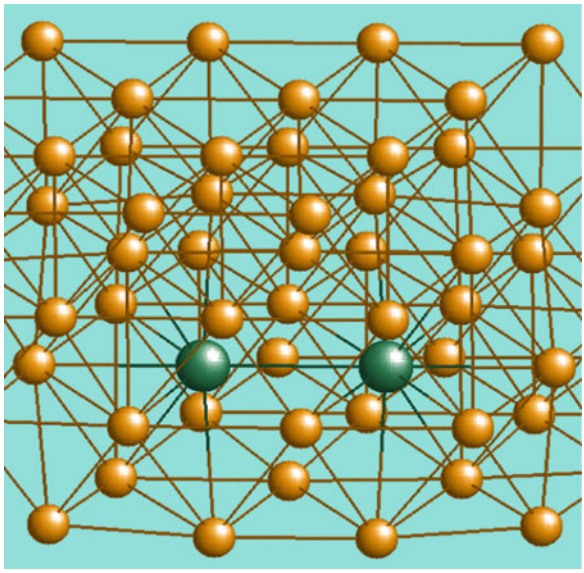

Fig. 14.1 Relaxed 1-NN configuration of Y-Y substitute atoms

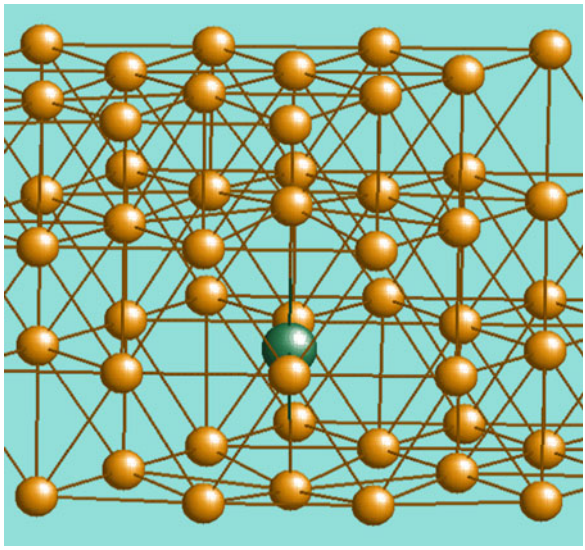

Fig. 14.2 Relaxed 1-NN configuration of Y-V_{Fe} pair

Qualitatively similar results of these calculations are shown in Tables 14.4 and 14.5, respectively. The largest binding energies have been obtained for pairs of atoms at 1-NN positions: 2.66 and 2.03 eV, respectively. With the increase of the inter-defect distance, the corresponding binding energies decrease. When the substitutes are located at 4-NN positions, their bonding has been found either very low (for Y-O pair) or even negative (for O-O pair). However, for both 4-NN types, the distance between the pair of atoms belonging to the same supercell is certainly larger than that between the same pairs of atoms arranged in adjacent supercells.

Table 14.1 Bonding in Y-Y pairs

Configuration	4 × 4 × 4 supercell E_{bind} (eV)
1-NN	−0.73
2-NN	−0.45
3-NN	−0.46
4-NN	−1.05

Table 14.2 Bonding in Y-V_{Fe} pairs

Configuration	4 × 4 × 4 supercell E_{bind} (eV)
1-NN	1.67
2-NN	−0.21
3-NN	0.30
4-NN	0.40

Table 14.3 Bonding in V_{Fe}-V_{Fe} pairs

Configuration	4 × 4 × 4 supercell E_{bind} (eV)
1-NN	0.25
2-NN	−0.09
3-NN	0.10
4-NN	−0.12

Table 14.4 Bonding in Y-O substitute pairs

Configuration	4 × 4 × 4 supercell E_{bind} (eV)
1-NN	2.66
2-NN	1.87
3-NN	1.27
4-NN	0.19

Table 14.5 Bonding in O-O substitute pairs

Configuration	4 × 4 × 4 supercell E_{bind} (eV)
1-NN	2.03
2-NN	1.63
3-NN	1.27
4-NN	-0.25

Table 14.6 presents the binding energies between Y substitute atom and O located in the octahedral interstitial site at various inter-atomic distances. Yttrium atom has been placed in the first, second and third coordination spheres around O atom. The negative binding energy has been calculated for 1-NN configuration of Y-O_{int} since the distance between the defect atoms is too small (certainly smaller than that in the equilibrium structure of Y and O atoms in any Y_2O_3 crystalline phase) which makes this configuration energetically unfavorable. The increase of Y-O_{int} distance results in the positive binding energy between impurity atoms. The binding energy is approximately the same in both cases, when Y is located in

Table 14.6 Bonding in Y-O_{int} pairs

Configuration	4 × 4 × 4 supercell E_{bind} (eV)
First coordination sphere	−0.21
Second coordination sphere	0.38
Third coordination sphere	0.42

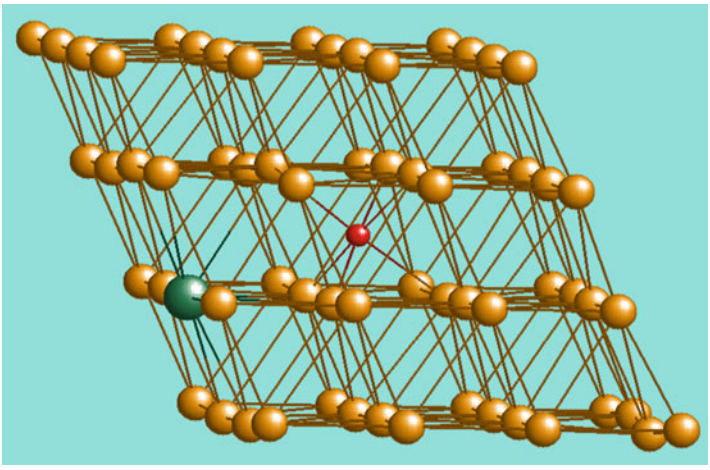

Fig. 14.3 Relaxed second coordination sphere for configuration of Y-O_{int} pair

Table 14.7 Triple-wise interactions in Y-O-Y and Y-V_{Fe}-Y clusters

Configuration	4 × 4 × 4 supercell E_{bind} (eV)
Y-O_{sub}-Y 2-NN	3.11
Y-O_{sub}-Y 1-NN	2.23
Y-O_{int}-Y	No bonding
Y-V_{Fe}-Y 2-NN	4.14

the second (Fig. 14.3) and the third coordination sphere around O_{int}, being equal to 0.38 and 0.42 eV, respectively, *i.e.*, substantially smaller than that for Y-O_{sub} pair (Table 14.5). Configuration of Y-O_{int} pair containing four coordination spheres around O_{int} cannot be completely arranged inside 4 × 4 × 4 γ-Fe supercell, this is why this configuration has not been calculated in this study.

Since the binding energy between the two yttrium substitutes has been always found to be negative, while other pairs consisting of impurity atoms and Fe vacancies are energetically stable, it has been suggested to add an oxygen atom positioned either at Fe vacancy or at the center of octahedral interstitial position to Y-Y pair, in order to construct a more stable cluster from solute impurity atoms. We have also removed a substitute O atom, to check the influence of the Fe vacancy on the binding energy between two yttrium atoms.

The results of calculations on triple-wise interactions between different combinations of impurity atoms and Fe vacancies are presented in Table 14.7.

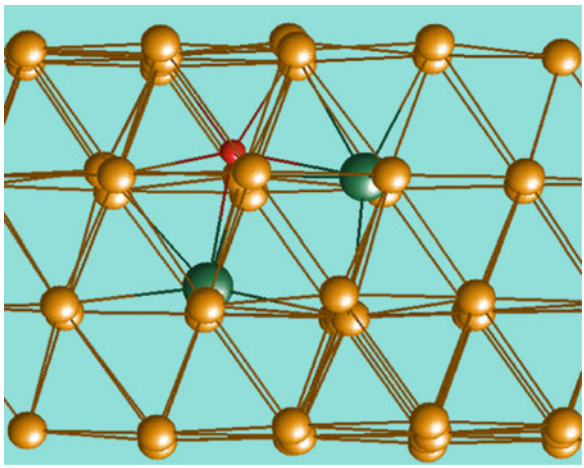

Fig. 14.4 Relaxed (*i*) configuration of 2Y-O substitute atoms

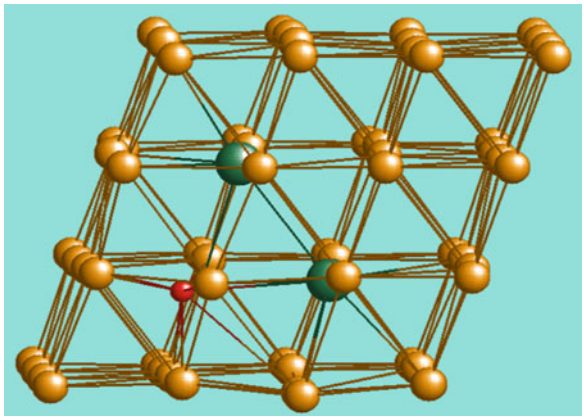

Fig. 14.5 Relaxed (*ii*) configuration of 2Y-O substitute atoms

Firstly, O atom has been positioned inside the Fe vacancy in two configurations of Y-O-Y cluster: (*i*) two substituted Y atoms are the next-nearest neighbors (2-NN) while O atom is the nearest neighbor (1-NN) for both Y atoms (Fig. 14.4); (*ii*) two substituted Y atoms are the nearest neighbors (1-NN) and O atom is the 1-NN neighbor to both Y atoms (Fig. 14.5). In (*i*) configuration, attraction between yttrium atoms has been observed, the initial distance between them decreases by 0.43 Å, whereas O atom is repelled from both Y atoms by 0.13 Å. In (*ii*) configuration, yttrium atoms repel from each other by 0.14 Å while the distance between both Y atoms and O atom increases by 0.24 Å. The calculated binding energies have been found to be quite high for both configurations (3.11 and 2.23 eV for (*i*) and (*ii*) configurations respectively). Thus, (*i*) configuration is energetically more favorable.

Calculations on Y-O_{int}-Y cluster containing two yttrium atoms at (*i*) 2-NN and (*ii*) 1-NN positions and O atom in the nearest interstitial position to both Y atoms (Figs. 14.6 and 14.7, respectively) have been also performed. For both these Y-O-Y

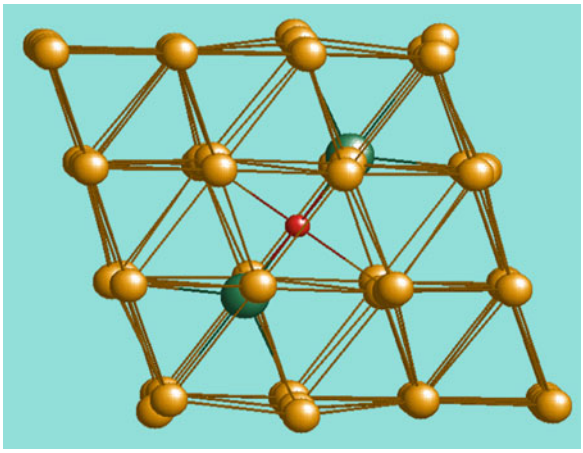

Fig. 14.6 Relaxed (*i*) configuration of 2Y-O_{int} atoms

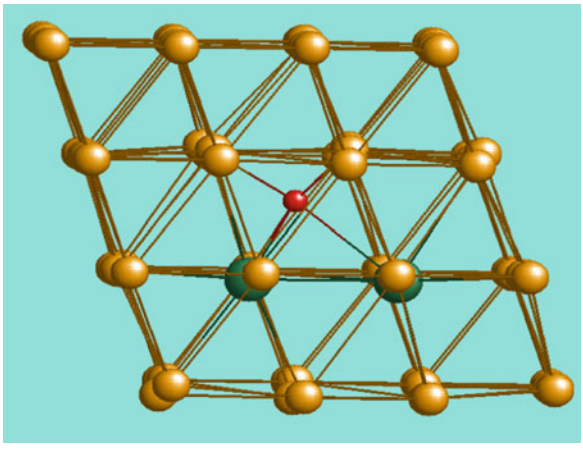

Fig. 14.7 Relaxed (*ii*) configuration of 2Y-O_{int} atoms

configurations, the negative binding energies have been found. Calculations on interstitial Y-O-Y configurations with a larger inter-atomic distance in each Y-O_{int} pair (analogously to those for pair-wise Y-O cluster described above) are in progress.

Energetically favorable Y-O-Y configuration shown in Fig. 14.4 has been also modified by removing O atom, in order to check the influence of Fe vacancy on the binding energy between two yttrium atoms. A certain attraction between two yttrium atoms (by 0.37 Å) has been observed. Table 14.7 clearly indicates that the binding energy in Y-V_{Fe}-Y cluster (4.14 eV) is even larger than in Y-O-Y cluster of the similar configuration which proves the importance of Fe vacancies during the formation of Y_2O_3 precipitates inside the γ-Fe lattice.

14.4 Conclusions

Large-scale first principles calculations have been performed for the γ-Fe lattice containing Y-Y, Y-V_{Fe}, V_{Fe}-V_{Fe}, Y-O and O-O pairs and different configurations of three-atom clusters - Y-O-Y and Y-V_{Fe}-Y. These calculations are required to accurately estimate the pair- and triple-wise interaction energies necessary for further lattice kinetic Monte Carlo (LKMC) simulations of ODS growth.

The analysis of the pair-wise interactions calculations shows that a certain attraction occurs between Y substitute atom and Fe vacancy, while no bonding occurs between two Y atoms at any distances. The calculations of the interactions between yttrium and oxygen substitute atoms as well as between two oxygen substitute atoms show a similar behavior with the highest binding energies at the distance of 1-NN and the decrease of the binding energy with the increase of the inter-defect distance. No significant bonding has been found between the two Fe vacancies located at different distances. At the same time, we can predict location of Fe vacancies in the proximity of impurity atoms

The calculations on different Y-O-Y cluster configurations clearly show that not only the presence of oxygen atom is required to form certain binding between impurity atoms but also the presence of Fe vacancies favors the growth of Y_2O_3 precipitates inside the iron crystalline matrix. This has been proved by the calculations of interactions inside the Y-V_{Fe}-Y cluster for which the binding energy has been found to be rather large.

Acknowledgements This work has been supported by European Social Fund project Nr. 2009/0202/1DP/1.1.1.2.0/09/APIA/VIAA/141, Euroatom-Latvia Fission and Euroatom Mobility Programs Technical assistance of Dmitry Bocharov and Sergey Piskunov is highly appreciated.

References

1. Lindau R, Möslang A, Rieth M, Klimiankou M, Materna-Morris E, Alamo A, Tavassoli A-AF, Cayron C, Lancha A-M, Fernández P, Baluc N, Schäublin R, Diegele E, Filacchioni G, Rensman JW, Van der Schaaf B, Lucon E, Dietz W (2005) Present development status of EUROFER and ODS-EUROFER for application in blanket concepts. Fusion Eng Design 75–79:989–996
2. Klimiankou M, Lindau R, Möslang A (2007) Direct correlation between morphology of $(Fe,Cr)_{23}C_6$ precipitates and impact behavior of ODS steels. J Nucl Mater 367–370:173–178
3. Lindau R, Möslang A, Schirra M, Schlossmacher P, Klimiankou M (2002) Mechanical and microstructural properties of a hipped RAFM ODS-steel. J Nucl Mater 307–311:769–772
4. Murty KL, Charit I (2008) Structural materials for Gen-IV nuclear reactors: challenges and opportunities. J Nucl Mater 383:189–195
5. Klimiankou M, Lindau R, Möslang A (2004) TEM characterization of structure and composition of nanosized ODS particles in reduced activation ferritic-martensitic steels. J Nucl Mater 329–333:347–351
6. Eiselt ChCh, Klimenkov M, Lindau R, Möslang A (2009) Characteristic results and prospects of the 13Cr–1W–0.3Ti–0.3Y_2O_3 ODS steel. J Nucl Mater 386–388:525–528

7. Okuda T, Fujiwara M (1995) Dispersion behaviour of oxide particles in mechanically alloyed ODS steel. J Mater Sci Lett 14:1600–1603
8. Odette GR, Alinger MJ, Wirth BD (2008) Recent developments in irradiation damage resistant steels. Ann Rev Mater Res 38:471–503
9. Miller MK, Kenik EA, Russell KF, Heatherly L, Hoelzer DT, Maziasz PJ (2003) Atom probe tomography of nanoscale particles in ODS ferritic alloys. Mater Sci Eng A 353:140–145
10. Klimenkov M, Lindau R, Möslang A (2009) New insights into the structure of ODS particles in the ODS-Eurofer alloy. J Nucl Mater 386–388:553–556
11. Gopejenko A, Zhukovskii YuF, Vladimirov PV, Kotomin EA, Möslang A (2010) Ab initio simulation of yttrium oxide nanocluster formation on fcc Fe lattice. J Nucl Mater 406:345–350
12. Gopejenko A, Zhukovskii YuF, Vladimirov PV, Kotomin EA, Möslang A (2011) Modeling of yttrium, oxygen atoms and vacancies in γ-iron lattice. J Nucl Mater 416:40–44
13. Kresse G, Hafner J (2007) VASP the guide. University of Vienna, Vienna. http://cms.mpi.univie.ac.at/vasp/
14. Kresse G, Furthmueller J (1996) Efficient iterative schemes for ab initio total-energy calculations using a plane-wave basis set. Phys Rev B 54:11169–11186
15. Perdew JP, Wang Y (1992) Accurate and simple analytic representation of the electron-gas correlation energy. Phys Rev B 45:13244–31249
16. Kresse G, Joubert D (1999) From ultrasoft pseudopotentials to the projector augmented-wave method. Phys Rev B 59:1758–1775